ONLINE SUPPLEMENT

Supplemental Methods

Cardiac fibroblast isolation and culture. Adult rat ventricular fibroblasts (ARVFs) were isolated from female Sprague Dawley rats using enzymatic digestion (1 mg/ml collagenase type II; Worthington Biochemical Corporation) followed by gentle centrifugation for collection of cells, as previously described [1]. Cells were maintained in DMEM/F12 media supplemented with 20% FBS, 1 % antibiotics-L glutamine and 1 μmol/L ascorbic acid. ARVFs were then passaged once to P1 (passage 1) or twice to P2 (passage 2), and plated appropriately for downstream assays. Equilibration of cells in low serum medium (0.1% FBS) was carried out prior to all treatments. Cells were treated with the following agents (DMSO as vehicle; 0.1% final concentration): recombinant TGF-β_1 (10ng/mL; Novoprotein, CA59), cyclosporin A (200nm; Sigma-Aldrich), JQ1 (500nM; synthesized in-house), SB203580 (10μM; Tocris), SP600125 (10μM; Selleckchem) or PD98059 (10μM; Selleckchem). For gene knockdown experiments using siRNAs, ARVFs were incubated with a transfection cocktail of siRNA (50nM; Sigma Aldrich) and Lipofectamine RNAiMAX reagent (Life Technologies) for eight hours, followed by removal of transfection complexes and treatment with TGF-β_1 for an additional 48 hours; siRNA sequences are provided in Supplemental Table 3. Lentiviral vector-mediated gene short-hairpin RNA (shRNA) knockdown experiments were performed by incubating ARVFs with lentivirus culture supernatants overnight, followed by equilibration with low-serum medium for an additional 24 hours prior to treatment with TGF-β_1. Cells were harvested for RNA, protein or chromatin analysis as appropriate. Adult mouse cardiac fibroblasts were also isolated from murine hearts post-TAC (± JQ1 *in vivo* treatment) treatment using enzymatic tissue dissociation (Liberase TH Research Grade; Roche), as described previously and with minor modifications [1, 2]. Cells were pre-plated for one hour followed by washing and isolation of total RNA and processed for RNA-seq.

Plasmids and lentivirus production. pLKO.1 plasmids (Sigma) encoding shRNA for *Sertad4* (TRCN0000247967 and TRCN0000247969) and a negative control (SHC002) were obtained through the Functional Genomics Facility at the University of Colorado Cancer Center. Lentiviruses were generated by co-transfecting L293 cells with pLKO.1 vectors in combination with packaging plasmid (psPAX2) and envelope plasmid (pMD2.G). Virus-containing cell culture supernatants were collected, filtered and used for experiments. psPAX2 and pMD2.G were gifts from Didier Trono (Addgene).

Collagen gel contraction assay. Compressible collagen matrices were prepared using PureCol EZ gel solution (5mg/mL; Advanced BioMatrix). ARVFs suspended in serum-supplemented DMEM/F-12 medium were seeded (5×10^4 cells/well) on collagen gels for 24 hours prior to equilibration by serum deprivation overnight. At the initiation of contraction, gels were released from wells and treated with DMSO (vehicle; 0.1% final concentration), TGF-β_1 (10ng/mL; Novoprotein, CA59) and/or JQ1 (500nM) for 72 hours. Well images were captured at 0, 24, 48 and 72 hours. Gel area for each well was determined using NIH ImageJ software and reported as percentage contraction.

Mouse transverse aortic constriction (TAC) model. All animal experiments were performed in accordance with the Institutional Animal Care and Use Committee at the University of Colorado Denver. Ten week-old male C57BL/6 mice (Jackson Laboratories) were subjected to sham or TAC surgery using a 27-gauge needle to guide suture constriction [3]; male mice were used because they respond more robustly to TAC than females [4]. JQ1 was delivered every other day via intraperitoneal injection at a concentration of 50mg/kg in a 1:4 DMSO:10% (2-Hydroxypropyl)-β-cyclodextrin (Sigma Aldrich; 389145) vehicle starting the day of TAC surgery. Animals were

randomly assigned to experimental groups using a constrained randomization method such that the same number of animals were included for each treatment group, each cage included animals from multiple groups, and any variations in weight were controlled. This was accomplished by an investigator distributing a list of animal numbers ranked by weight, moving down the list 4 animals at a time and distributing the animals into groups A, B, C, D randomly though without allowing the same group to receive multiple assignments within the block of 4 animals. The distribution was checked following assignment to ensure that each cage had multiple groups assigned. Animals and samples were assigned an alphanumeric designation for blinding, and the surgeon was blinded to the treatment groups. Sample sizes were based on prior determination by our laboratory of the number of mice needed to see a significant increase in LV hypertrophy post-TAC. Two animals did not respond as expected based on HW/TL measurements (1 TAC and 1 TAC/JQ1). These animals were not included for RNA-seq analysis. Though not determined a priori, exclusion was justified given the intent to uncover novel BET protein mediated biology of pathologic cardiac remodeling (as indicated by HW/TL).

Mass spectrometry. Total protein was harvested from cardiac fibroblasts (three biological replicates) treated with DMSO (vehicle; 0.1% final concentration), TGF-β_1 (10ng/mL; Novoprotein, CA59) and/or JQ1 (500nM) using Mammalian Protein Extraction Reagent (M-PER; Thermo Scientific) and sonication (Fisher Scientific FB120). Protein concentration was determined using a bicinchoninic acid assay (Thermo Scientific). The samples (50µg) were digested using a filter-assisted sample preparation (FASP)/trypsin protocol. The digested peptides were fractionated using a high-pH reversed phase (RP) peptide fractionation kit (Thermo Scientific). Fractions collected from the high-pH RP fractionation were further separated using on-line second-dimension low-pH reversed-phase chromatography via an Easy-nLC 1200 nanoflow-UHPLC system (Thermo Scientific) on an EasySpray C18 column (PepMap RSLC C18, 3-µm particle,

100-Å pore; 75 µm x 15 cm dimension; Thermo Scientific) held at 45°C. The typical solvent gradient was 0–80 min: 0–35% B; 80–85 min: 35–100% B; 85–90 min: 100% B; 300 nL·min-1; Solvent A: 0.1% formic acid in water; Solvent B: 80% acetonitrile, 0.1% formic acid in water. 4 µL of each high-pH fraction was injected by the autosampler on the Easy-nLC 1200 nanoflow-UHPLC system. The eluent from the Easy-nLC system was analyzed using a Q-Exactive HF Hybrid Quadrupole-Orbitrap mass spectrometer (Thermo Scientific) coupled online to the nanoflow-UHPLC through a Thermo EasySpray ion source. Acquired mass spectra were centroids and converted to .mzML formats using ProteoWizard msConvert [5]. Database search was performed using a modified SEQUEST algorithm implemented in Comet (Crux version 3.0 distribution) [6] with a concatenated decoy search against a *Rattus norvegicus* proteome database (TrEMBL and Swiss-Prot) retrieved on 2017/10/19 with 29,979 entries from http://uniprot.org [7]. False discovery rate (FDR) analyses were performed by Percolator (Crux version 3.0) [8], requiring < 1% global peptide false discovery rate (Percolator q < 0.01) for a peptide and protein to be identified and quantified. Normalized spectral abundance factor (NSAF) values (calculated using peptides with Percolator q < 0.01) were calculated for protein quantification. Comparisons between the sample groups were performed using limma [9] in R/Bioconductor [10] with a moderated t-test using NSAF values. Technical replicate (two each) values were averaged prior to limma analysis. Proteomics data used for principal component analysis (PCA) were preprocessed by dividing protein NSAF values by the average of the three vehicle biological replicates. Proteins from the treatment groups vehicle, TGF-β, and TGF-β +JQ1 that were shown to be induced by TGF-β (Benjamini & Hochberg adjusted *P*-value ≤ 0.1) were extracted, $\log_2$ transformed, clustered, and plotted as a heat map using R. Proteomics data are deposited in the PRIDE Archive (https://www.ebi.ac.uk/pride/archive/login). The accession number for the dataset is PXD012482. Username: reviewer64803@ebi.ac.uk; Password: vqYL216E.

All peptides used in the calculation of the periostin NSAF values were uniquely mapped to periostin. In total, 3066 proteins without any missing data across all replicates and treatments were included in the PCA analysis. The PCA analysis is based on quantitative expression. PCA was performed using R version 3.4 and the principal component analysis function (prcomp) from its stat package. Normalized spectral abundance factor (NSAF) values calculated using Crux version 3.0 for each treatment were provided as inputs. The heatmap was generated using the Hierarchical Clustering function (hclust) from the stat package and ggplot2 from R version 3.4. Colors in the heatmap were generated by R version 3.4 after standardizing the NSAF values from each treatment group through the scale function in R. Relatively up-regulated values are depicted in red and relatively down-regulated values are displayed in blue, with a range of ~2 (red) to -2 (blue).

Quantitative real-time PCR (qRT-PCR). Total RNA was collected from cells using QIAzol lysis reagent (Qiagen) and used for cDNA synthesis (Verso cDNA Synthesis Kit; Life Technologies). Gene expression was assayed on a StepOnePlus Real-Time PCR (Applied Biosystems) using the PowerUp SYBR Green Master Mix (Applied Biosystems). Amplicon abundance was quantified using the $2^{-\Delta\Delta Ct}$ method. Primer sequences are listed in Table S1.

RNA-seq analysis. Total RNA was prepared from fibroblasts isolated from mouse hearts using Direct-zol RNA miniprep kit (Zymo Research). cDNA libraries were prepared using the NEBNext Ultra Directional Library Preparation Kit following rRNA depletion using the NEB rRNA depletion kit. Libraries were submitted to the UC Denver Genomics and Microarray core facility for sequencing (HiSeq2000). Reads were trimmed with Trim Galore! (v.0.3.7) and aligned with STAR (v.2.5.2a) [11] to the mouse genome (Mm10) with annotations from UCSC (July 2016). Raw counts were loaded in to R [12]. Genes with a median of <1 mapped read per million were removed before differential expression analysis with edgeR [13].

For RNA-seq analysis of ARVFs, cells were treated with DMSO (vehicle; 0.1% final concentration), TGF-β_1 (10ng/mL) and/or JQ1 (500nM). Total RNA was isolated using the Direct-zol RNA miniprep kit (Zymo Research). cDNA libraries were prepared using the NEBNext Ultra Directional RNA Library Prep Kit for Illumina following PolyA selection. Samples were submitted to WIGTC for sequencing (HiSeq 2500). All analyses were performed using the Rat RN6 genome and RN6 RefSeq gene annotations. All RNA-seq datasets were aligned to the transcriptome using Tophat2 (version 2.0.11) (http://www.genomebiology.com/2013/14/4/R36/abstract). Gene expression values were quantified using Cufflinks and Cuffnorm, and differential expression was determined with Cuffdiff (version 2.2.0) [14]. Heatmaps were generated using pheatmap v.1.0.8 [15]. Row-normalized values range from -2 to 2. Genes were clustered by correlation in pheatmap. The GEO accession number for RNA-seq data is GSE127229. The publication series accession number is GSE127230.

Congruency analysis: Direct comparison between DE gene lists from different experiments, especially across platforms (mass spec., RNA-seq) is prone to missed concordances. Gene set enrichment analysis (GSEA, Broad Institute), which more sensitively identifies trends, was therefore run to compare similarities in gene expression and protein expression programs in cultured ARVFs stimulated with TGF-β, and again comparing these to gene expression programs in resident cardiac fibroblasts of mice subjected to TAC. For these comparisons, lists of genes/proteins found to be significantly upregulated or downregulated were analyzed for enrichment, with comparison datasets pre-ranked by log2 fold change. For example, in Online Figure IVA, the list of proteins found to be significantly upregulated by TGF-β stimulation in mass spectrometry analysis (Figure 3) were compared against the entire list of genes from ARVF RNA-seq pre-ranked by log2 fold change following TGF-β stimulation. The majority of the increased proteins were found at or near the top of the ranked RNA-seq dataset, indicating significant enrichment, as supported by an FDR q-value <1e-3.

ChIP-seq and ChIP-PCR. Anti-BRD4 (301-985, Bethyl Laboratories) and anti-RNA Pol II (39097, Active Motif) Chromatin Immunoprecipitation was performed as previously described [16]. Five independent 10-cm plates of ARVFs were combined per immunoprecipitation. Libraries were prepared using the Rubicon TruPLEX Tag-seq kit and submitted to the UC Denver Genomics and Microarray core facility for sequencing (HiSeq2000). For validation of BRD4-bound enhancers or super-enhancers of the *Sertad4* locus, ChIP was performed as described above. The immunoprecipitates were collected and eluted DNA was subjected to qPCR using specific primers (Integrated DNA Technologies; primer sequences are listed in Table S2.

All ChIP-seq datasets were aligned using Bowtie2 (version 2.2.1) to build version RN4 of the rat genome [17]. Alignments were performed using the following criteria: -k 1. These criteria preserved only reads that mapped uniquely to the genome. ChIP-seq read densities were calculated and normalized using Bamliquidator (https://github.com/BradnerLab/pipeline/wiki/Bamliquidator). Briefly, ChIP-seq reads aligning to the region were extended by 200 base pairs (bp) and the density of reads per bp was calculated. The density of reads in each region was normalized to the total number of million mapped reads producing read density in units of reads per million mapped reads per bp (rpm/bp). MACS version 1.4.2 (model-based analysis of ChIP-seq) peak finding algorithm was used to identify regions of ChIP-seq enrichment over background [18]. A *P*-value threshold of enrichment of 1e-9 was used for all datasets. A gene was defined as actively transcribed if enriched regions for RNA Pol II were located within 1 kb in either direction of the TSS and FPKM >10 cutoff in at least one sample. The GEO accession number for ChIP-seq data is GSE127214.

Mapping and comparing enhancers and super-enhancers. BRD4 ChIP-seq data were used to identify active *cis*-regulatory elements in the genome. ROSE2 (https://github.com/bradnerlab/pipeline/) was used to identify BRD4 enhancers and super-

enhancers, as previously described [19]. Briefly, proximal regions of BRD4 enrichment were stitched together if within 2 kb of one another. This 2 kb stitching parameter was determined by ROSE2 as the distance that optimally consolidated the number of discreet enriched regions in the genome while maintaining the largest fraction of enriched bases per region. Comparison of BRD4 changes at enhancers, super-enhancers, and promoter regions was performed as previously described [19]. Active genes, defined by presence of RNA Pol II in the TSS +/- 1 kb region, within 50 kb of enhancer regions were assigned as target genes, as described previously [19]. Promoters for heat maps were identified by overlapping TSS -/+ 1,000 bp regions with peaks from treated and unstimulated BRD4 ChIP-seq data. Enhancer and promoter heat map figures were generated by combining three separate heat maps made from partitions of all the enhancers identified in the unstimulated and stimulated samples and all of the promoters identified in the unstimulated and stimulated samples. The partitions consisted of conserved regions (appearing in both states), lost regions (appearing only in the unstimulated state), and gained regions (appearing only in the stimulated state). Enhancers were assigned to an active gene if the gene TSS was within +/- 50kb of the enhancer center. Median normalization was applied prior to taking the log2 fold change only for comparing RNA Pol II occupancy in Figure 5D. The mRNA data in Figure 5C were drawn from FPKM values processed by the cufflinks pipeline which includes a normalization step (Cuffnorm). For figure 5D, for each dataset (+TGF-β or vehicle), the RNA Pol II occupancy was first divided by the median signal across all active genes.

Indirect immunofluorescence. ARVFs were cultured on 96-well clear-bottom plates (Greiner, 655090); each well received 350 cells in 100 µL of Fibroblast Growth Media (Lonza, CC-3131) supplemented with FGM-2 SingleQuots (Lonza, 4126). The following day, cells were washed with Fibroblast Growth Media (without FGM-2) supplemented with penicillin-streptomycin. After incubation with DMSO or JQ1 for 1 hour, TGF-β_1 (10ng/mL; PeproTech, 100-21C) was added to

cells for 72 hours prior to fixation with 100% methanol (Fisher) at -20ºC. Fixed cells were washed and incubated with primary antibodies as a cocktail (1:2000 anti-α-SMA, Abcam, ab7817; 1:200 anti-fibronectin, Abcam, ab2413) overnight at 4ºC. Cells were washed and incubated with a cocktail of secondary antibodies (1:400 goat anti-mouse Alexa488, Thermo; 1:400 goat anti-rabbit Alexa647, Thermo; 1:2000 Hoechst 33342, Thermo), and incubated for one hour in the dark. Imaging was performed on a CellInsight CX7 HCS plate reader (Thermo). This assay was validated using appropriate negative controls to include fibroblast wells lacking primary antibody incubation.

For quantification of effects of BET family member knockdown on α-SMA protein expression, ARVFs seeded on glass coverslips were incubated with a transfection cocktail of siRNA (50nM; Sigma Aldrich) and Lipofectamine RNAiMAX reagent (Life Technologies) for eight hours. Following removal of transfection complexes, cells were treated with TGF-β_1 (10ng/mL; Novoprotein, CA59) for an additional 48 hours. Cells were then fixed with ice-cold methanol (Fisher) at -20ºC, followed by washing and incubation with anti-α-SMA antibody (Abcam; 1:2000) at 4ºC overnight. Coverslips were then rinsed, incubated with goat anti-mouse Alexa488 (Thermo; 1:1000) and nuclei were counterstained using Hoechst 33342 (Thermo; 1µg/mL). Cells on coverslips were washed and mounted on glass slides using ProLong™ Glass Antifade Mountant (Thermo) and allowed to cure for 24 hours prior to imaging. Images were obtained using a 20x objective on a Keyence BZ-X800 fluorescence microscope using appropriate filters. αSMA protein intensity was quantified using RGB measurement tool in ImageJ software (NIH) and normalized to total cell numbers.

Immunoblotting. Total protein was isolated from ARVFs using RIPA lysis buffer (50mM Tris-HCl pH 8.0, 150mM NaCl, 1% NP40, 0.5% sodium deoxycholate, 0.1% SDS) supplemented with protease and phosphatase inhibitor cocktail (Thermo Fisher Scientific). Proteins were separated

using SDS-PAGE and transferred onto nitrocellulose membranes (0.45µm; Life Science Products). Blots were probed with primary antibodies specific for BRD2 (Cell Signaling; 5848), BRD3 (Santa Cruz Biotechnology; sc-75630), BRD4 (Bethyl Laboratories; A301-985A100) or α-tubulin (Santa Cruz Biotechnology; sc-23948) overnight at 4°C. Following incubation with primary antibodies, blots were rinsed and probed with appropriate HRP-conjugated mouse or rabbit secondary antibodies (Southern Biotech). Protein bands were visualized using enhanced chemiluminescent HRP substrate (SuperSignal West Pico Chemiluminescent Substrate; Thermo Scientific) on a FluorChem HD2 Imager (Alpha Innotech), and band intensities were quantified using Quantity One analysis software (Bio-Rad).

Viability and proliferation assessment. ARVF viability was determined using a FITC Annexin V/Dead Cell Apoptosis Kit (Thermo Fisher Scientific; V13242) following the manufacturer's instructions. This product detects the externalization of phosphatidylserine in apoptotic cells using recombinant annexin V conjugated to green-fluorescent FITC dye, as well as dead cells using propidium iodide (PI), which is impermeant to live and apoptotic cells. These populations were distinguished using a Beckman Coulter Gallios flow cytometer with the 488 nm line of an argon-ion laser for excitation. Cell proliferation was determined as an endpoint cell number determination using the data derived from the 96-well plate-based indirect immunofluorescence method described above. Cell numbers were derived from the total Hoechst 33342 stained nuclei found in nine image fields for each well. Data were normalized to the nuclei counts in the no TGF-β treatment controls wells (8-wells per plate).

Ingenuity Pathway Analysis. Following differential gene expression analysis of RNA-seq data detailed above, core analyses were accomplished in IPA to identify affected pathways and candidate upstream regulators by comparing gene expression in sham to TAC fibroblasts, and

again for TAC to TAC plus JQ1 treatment (FC>+1.5 or FC<-1.5, FDR <0.1). Similarly, differential expression data from the Cuffdiff analysis was used to compare gene expression programs in vehicle to TGF-β treated fibroblasts (log_2 FC>1 or log_2<-1, minimum expression 10 fpkm, and FDR <0.1) and again for TGF-β to TGF-β plus JQ1 treated fibroblasts, (log_2 FC>0.5 or log_2 FC<-.05, minimum expression 10 fpkm, and FDR<0.1). The top 5 canonical pathways significantly altered in a given analysis were reported as "Affected pathways" with *P*-values listed from Fisher's exact test, right tailed. This analysis option is found in the "canonical pathways" tab within IPA. For Figure 2C and 2D, and again in Figure 3D, genes with expression changes that led to IPA identifying a particular upstream effector molecule (TGF-β, Figure 2) or pathway (hepatic fibrosis, Figure 3) were displayed with color indicating strength and direction of expression change (no color if expression change did not meet the above criteria). For illustration purposes in Figure 2C, the mechanistic network for TGF-β in the analysis was displayed. Then target genes (table provided below the network in IPA) were added to the network. Next, network hubs were deleted (hence some molecules without direct lines from TGF-β). Finally, reduced genes were deleted and induced genes were manually placed to allow visualization. Representation of the same genes to reflect changes from the insult to insult +JQ1 analysis (Figure 2D and Figure 3D) was accomplished using the "build" and "grow" options in the Path Designer tool. Length of arrows or line segments do not encode any information.

Statistical Analysis. qRT-PCR, ChIP-PCR, immunoblotting, immunofluorescence, viability, proliferation, and gel contraction data were analyzed using GraphPad Prism (version 7.03 for Windows). Several analyzed sample groups did not fit normal distribution for particular measurements as tested using the Shapiro-Wilk test. These were found in Fig. 1J (siCtrl), Fig. 6G (JQ1), Fig. 7B (p38i), Fig. 7C (TGF-β/p38i), Fig 7E (E3, p38i) and Fig 8A (shSertad4 (#1)/TGF-β). If non-normal distribution was found in a sample group that was not of post hoc interest (e.g. Fig 1J siCtrl), the Kruskal-Wallis test (designed for non-parametric data) was used to determine

if means across the groups were significantly different before reporting ANOVA associated post hoc test results. When non-normal distribution was found in a sample group of post hoc interest, the Mann-Whitney test (two-tailed) was implemented following significant ($p<0.05$) Kruskal-Wallis test as needed. Specific statistical tests employed are detailed in the figure legends. In cases where multiple independent variables were present, additional two-way ANOVAs were performed to inform relative contributions of the independent variables. Multiple tools were used in the analysis of ChIP-Seq, RNA-Seq and Mass Spectrometry data and are indicated above for each method.

Online Table I. Primers for qPCR

Target	5' oligo	3' oligo
Brd2	AGCACCAGGGAAAAGGATTC	GATGCTTCCACAGAGCCTTC
Brd3	CTCCCCCACCTGAGGTCT	AGGCAGGTTCAGCTTGATTG
Brd4	CCCTGGGACAAGATTGAGAA	CTGCCTCTTGGGCTTGTTAG
B2M	TCACACCCACCGAGACCGATGT	TCTCGGTCCCAGGTGACGGTTT
Sertad4	GGTAAGTTCTCCCACTTTCTCC	TGCCCAAACGATCTACTCATAC
αSMA	GGAGATGGCGTGACTCACAA	CGCTCAGCAGTAGTCACGAA
Periostin	TCGTGGAACCAAAAATTAAAGTC	CTTCGTCATTGCAGGTCCTT

Online Table II. Primers for ChIP-qPCR

Target	5' oligo	3' oligo
Sertad4 Enh/SE 1	CAAATGCTGGGAATCTGAACTG	TTAGGCCCTTCTGTCCTATCT
Sertad4 Enh/SE 2	CCACTTCAGAGACAAGCTCTTT	CACAGACTAGGTTGAGCATTCC
Sertad4 Enh 3	CACTACCGCCACTTACCTTTC	GGCGACTTCTCTGAAACCAATA
Sertad4 Enh 4	ACAGTGCCAGAGTCCAAAC	CTCTGATGGTGCTGACCTATTT
Sertad4 Enh 5	TTCGGGCATCCGTTCAAA	TGCTTGGAGCGCTTTCTTA
Sertad4 Enh 6	CAGGGCTGGAAGGAAAGTAAA	CGAGGTTTATGGCGGGATTAG
Sertad4 TSS	CAGTGCCTCTCCTGAAGAATAA	GGCGTGTGTTTCCCATAGA

Online Table III. siRNA sequences

Target	Genbank Accession#	siRNA ID	Sense oligo	Antisense oligo
BRD2	NM_212495	270473	CUGUCAAGCGGAAGAU GGAdTdT	UCCAUCUUCCGCUUGA CAGdTdT
BRD3	NM_001108575	239989	GUGCUAAUGGCCCAG GCCUdTdT	AGGCCUGGGCCAUUA GCACdTdT

BRD4	XM_001065925	315747	GACAUGAGCACAAUCA AGUdTdT	ACUUGAUUGUGCUCAU GUCdTdT

Online Table IV. Differential effects of TGF-β and JQ1 on ARVF gene expression

Online Table V. Gene and protein expression comparisons following pro-fibrotic stimulus

Supplemental Figure Legends

Online Figure I. JQ1 suppresses proliferation induced by TGF-β. A, ARVFs were cultured on a 96-well plate and stimulated with TGF-β for 72 hours. TGF-β-stimulated cell proliferation was assessed by counting total stained nuclei from nine image fields in eight wells/treatment group for ARVF treated with or without TGF-β. The data are normalized to the mean nuclei count in the untreated wells and the data are presented as mean ± SEM. *P< 0.05 vs. the no TGF-β control wells. **B**, JQ1 was tested in concentration response format (10μM to 5nM final concentration) for the ability to block TGF-β stimulated ARVF proliferation. Each concentration was tested in duplicate wells and the data for total stained nuclei were normalized to the untreated control wells of the plate. The IC_{50} for inhibition of proliferation was determined by non-linear regression of the normalized data. **C**, ARVFs were cultured on 100-mm plates and left untreated or exposed to DMSO vehicle, JQ1 (500 nM), TGF-β or TGF-β plus JQ1 for 48 hours. A viability assay was performed using annexin V and propidium iodide to determine the number of apoptotic and dead cells, respectively.

Online Figure II. JQ1 suppresses pro-fibrotic gene expression in cardiac fibroblasts. ARVFs were treated with DMSO vehicle, JQ1, TGF-β, or TGF-β plus JQ1 for 24 hours prior to extraction of RNA for RNA-seq analysis. **A**, Heat map of genes significantly altered by TGF-β

treatment. Each column represents data from a distinct plate of cells. **B**, Ingenuity pathway analysis (IPA) was used to determine canonical pathways significantly associated with distinct gene sets based on responses to TGF-β and JQ1 (red block = JQ1 blunted TGF-β dependent activation; blue block = JQ1 augmented TGF-β dependent activation; grey block = TGF-β reduced genes that are activated by JQ1 alone; black block = TGF-β and JQ1 reduced genes). Gene lists for members of red, blue, grey, and black blocks are available in Online Table IV.

Online Figure III. JQ1 suppresses pressure overload-induced pro-fibrotic gene expression in cardiac fibroblasts *in vivo*. **A**, Mice were subjected to Sham surgery or transverse aortic constriction (TAC), and were treated with JQ1 or vehicle control for two weeks. TAC triggered cardiac hypertrophy, which was normalized by JQ1. Data are presented as mean ± SEM; *P<0.05 vs all other groups by one-way ANOVA with Tukey's post-hoc test. **B**, Heat map of resident cardiac fibroblast transcripts that were significantly upregulated by TAC and suppressed by JQ1. Samples from Sham operated mice treated with JQ1 are also included (related to Figure 3B). Consistent with the ability of JQ1 to block TAC-induced pro-fibrotic gene expression, the TAC + vehicle samples were the only clearly segregated samples following unsupervised clustering, while the TAC + JQ1 samples were interspersed with Sham + vehicle and Sham + JQ1 samples.

Online Figure IV. Similar gene expression programs are induced in response to TGF-β in cultured ARVFs and in resident cardiac fibroblasts in mice subjected to TAC. Subsequent to species mRNA:mRNA and mRNA:protein identifier matching, gene set enrichment analysis was used to determine congruency between mRNAs and proteins induced by TGF-β **(A)**, mRNAs and proteins repressed by TGF-β **(B)**, mRNAs induced by TGF-β and TAC **(C)**, mRNAs repressed by TGF-β and TAC **(D – not significant)**, proteins induced by TGF-β and mRNAs induced by TAC **(E)**, proteins repressed by TGF-β and mRNAs repressed by TAC **(F – not significant)**, and

JQ1 targets in TGF-β and TAC induced mRNAs **(G)**. Ingenuity Pathway Analysis (IPA) was used to determine canonical pathways specifically associated with enriched genes/proteins in each analysis (even if overall enrichment was not significant – **D**, **F**), and are reported below the enrichment plots. Detailed GSEA results for each analysis are available in Online Table V.

Online Figure V. Binding of BRD4 to cardiac fibroblast promoters. ARVFs were employed for ChIP-seq analysis, as described in Figure 4. Shown is a heat map of BRD4-bound promoters in TGF-β and unstimulated ARVFs covering 1kb upstream and downstream of the transcription start site (TSS); mean reads per million mapped reads per base pair (RPM/bp). Promoters are grouped by gain, loss, or conservation in TGF-β stimulated ARVFs and ranked in order of decreasing BRD4 binding in unstimulated ARVFs in each group.

Online Figure VI. BRD4 and RNA Pol II binding to α-SMA and periostin regulatory elements in cardiac fibroblasts. Gene tracks showing BRD4 and RNA Pol II binding to the *Acta2* and *Postn* gene loci in ARVFs in the absence or presence of TGF-β stimulation, as schematized in Figure 5A. TGF-β stimulation led to a modest increase in BRD4 binding to *Postn* gene regulatory elements.

Supplemental References

1. Bagchi RA, Roche P, Aroutiounova N, Espira L, Abrenica B, Schweitzer R and Czubryt MP. The transcription factor scleraxis is a critical regulator of cardiac fibroblast phenotype. *BMC Biol*. 2016;14:21.

2. Lighthouse JK, Burke RM, Velasquez LS, Dirkx RA, Jr., Aiezza A, 2nd, Moravec CS, Alexis JD, Rosenberg A and Small EM. Exercise promotes a cardioprotective gene program in resident cardiac fibroblasts. *JCI Insight*. 2019;4.

3. Spiltoir JI, Stratton MS, Cavasin MA, Demos-Davies K, Reid BG, Qi J, Bradner JE and McKinsey TA. BET acetyl-lysine binding proteins control pathological cardiac hypertrophy. *J Mol Cell Cardiol*. 2013;63:175-9.

4. Fliegner D, Schubert C, Penkalla A, Witt H, Kararigas G, Dworatzek E, Staub E, Martus P, Ruiz Noppinger P, Kintscher U, Gustafsson JA and Regitz-Zagrosek V. Female sex and estrogen receptor-beta attenuate cardiac remodeling and apoptosis in pressure overload. *Am J Physiol Regul Integr Comp Physiol*. 2010;298:R1597-606.

5. Adusumilli R and Mallick P. Data Conversion with ProteoWizard msConvert. *Methods Mol Biol*. 2017;1550:339-368.

6. Eng JK, Hoopmann MR, Jahan TA, Egertson JD, Noble WS and MacCoss MJ. A deeper look into Comet--implementation and features. *J Am Soc Mass Spectrom*. 2015;26:1865-74.

7. UniProt C. UniProt: a hub for protein information. *Nucleic Acids Res*. 2015;43:D204-12.

8. The M, MacCoss MJ, Noble WS and Kall L. Fast and Accurate Protein False Discovery Rates on Large-Scale Proteomics Data Sets with Percolator 3.0. *J Am Soc Mass Spectrom*. 2016;27:1719-1727.

9. Ritchie ME, Phipson B, Wu D, Hu Y, Law CW, Shi W and Smyth GK. limma powers differential expression analyses for RNA-sequencing and microarray studies. *Nucleic Acids Res*. 2015;43:e47.

10. Huber W, Carey VJ, Gentleman R, Anders S, Carlson M, Carvalho BS, Bravo HC, Davis S, Gatto L, Girke T, Gottardo R, Hahne F, Hansen KD, Irizarry RA, Lawrence M, Love MI, MacDonald J, Obenchain V, Oles AK, Pages H, Reyes A, Shannon P, Smyth GK, Tenenbaum D, Waldron L and Morgan M. Orchestrating high-throughput genomic analysis with Bioconductor. *Nat Methods*. 2015;12:115-21.

11. Dobin A, Davis CA, Schlesinger F, Drenkow J, Zaleski C, Jha S, Batut P, Chaisson M and Gingeras TR. STAR: ultrafast universal RNA-seq aligner. *Bioinformatics*. 2013;29:15-21.

12. Team RC. R: A Language and Environment for Statistical Computing. . *https://wwwR-projectorg/*. 2017.

13. Robinson MD, McCarthy DJ and Smyth GK. edgeR: a Bioconductor package for differential expression analysis of digital gene expression data. *Bioinformatics*. 2010;26:139-40.

14. Trapnell C, Williams BA, Pertea G, Mortazavi A, Kwan G, van Baren MJ, Salzberg SL, Wold BJ and Pachter L. Transcript assembly and quantification by RNA-Seq reveals unannotated transcripts and isoform switching during cell differentiation. *Nat Biotechnol*. 2010;28:511-5.

15. Kolde R. pheatmap: Pretty Heatmaps. R package version 1.0. 8.

16. Stratton MS, Lin CY, Anand P, Tatman PD, Ferguson BS, Wickers ST, Ambardekar AV, Sucharov CC, Bradner JE, Haldar SM and McKinsey TA. Signal-Dependent Recruitment of BRD4 to Cardiomyocyte Super-Enhancers Is Suppressed by a MicroRNA. *Cell Rep*. 2016;16:1366-1378.

17. Langmead B and Salzberg SL. Fast gapped-read alignment with Bowtie 2. *Nat Methods*. 2012;9:357-9.

18. Zhang Y, Liu T, Meyer CA, Eeckhoute J, Johnson DS, Bernstein BE, Nusbaum C, Myers RM, Brown M, Li W and Liu XS. Model-based analysis of ChIP-Seq (MACS). *Genome Biol*. 2008;9:R137.

19. Brown JD, Lin CY, Duan Q, Griffin G, Federation A, Paranal RM, Bair S, Newton G, Lichtman A, Kung A, Yang T, Wang H, Luscinskas FW, Croce K, Bradner JE and Plutzky J. NF-kappaB directs dynamic super enhancer formation in inflammation and atherogenesis. *Mol Cell*. 2014;56:219-231.

Online Figure I

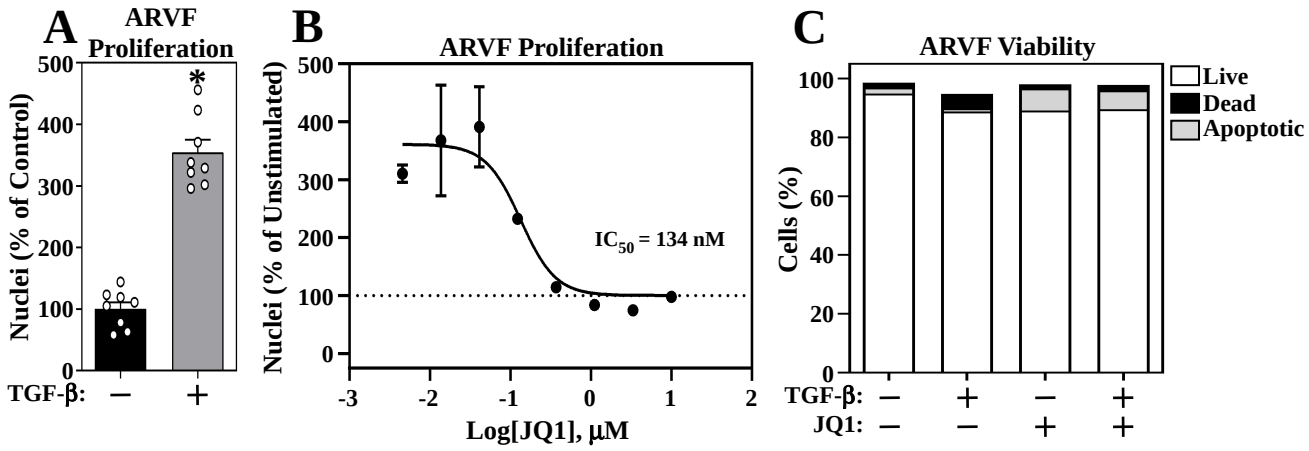

Online Figure II

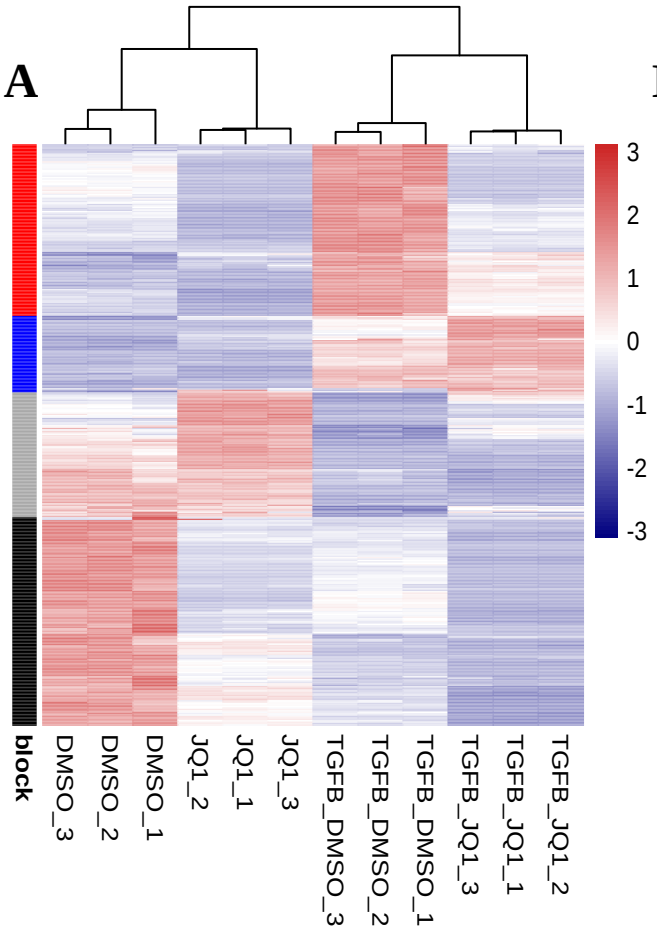

B

Remodeling of Epithelial Adherens Junctions, p=3.27 E-05, overlap = 7.2%
Colanic Acid building Blocks Biosynthesis, p=5.05 E-05, overlap = 21.4%
Glycolysis I, p=3.44 E-04, overlap = 11.5%
Gluconeogenesis I, p=3.44 E-04, overlap = 11.5 %
Oleate Biosynthesis II, p=2.09 E-03, overlap = 15.4%

Retinoate Biosynthesis I, p=3.13 E-03, overlap = 5.9%
Putrescine Biosynthesis III, p=4.88 E-03, overlap = 50.0%
NADH Repair, p=7.31 E-03, overlap = 33.3%
Retinoate Biosynthesis II, p=9.74 E-03, overlap =25.0%
Pentose Phosphate Pathway (Oxidative Branch), p=9.74 E-03, overlap = 25.0%

Mouse Embryonic Stem Cell Pluripotency, p= 3.65 E-06, overlap = 5.1%
Regulation of the Epithelial-Mesenchymal Transition Pathway, p=7.83 E-05, overlap = 3.0%
Osteoarthritis Pathway, p=1.05 E-04, overlap = 2.8%
AMPK Signaling, p=1.49 E-04, overlap = 2.7%
Human Embryonic Stem Cell Pluripotency, p=1.74 E-04, overlap = 3.4%

LPS/IL-1 Mediated Inhibition of RXR Function, p=1.06 E-5, overlap = 4%
Cell Cycle: G2/M DNA Damage Checkpoint Regulation, p=2.35 E-04, overlap = 8.2%
Estrogen-mediated S-Phase Entry, p=5.34 E-04, overlap = 11.5%
Mitotic Roles of Polo-Like Kinase, p=7.36 E-04, overlap = 6.1%
Glioma Signaling, p=1.07 E-03, overlap = 4.0%

Online Figure III

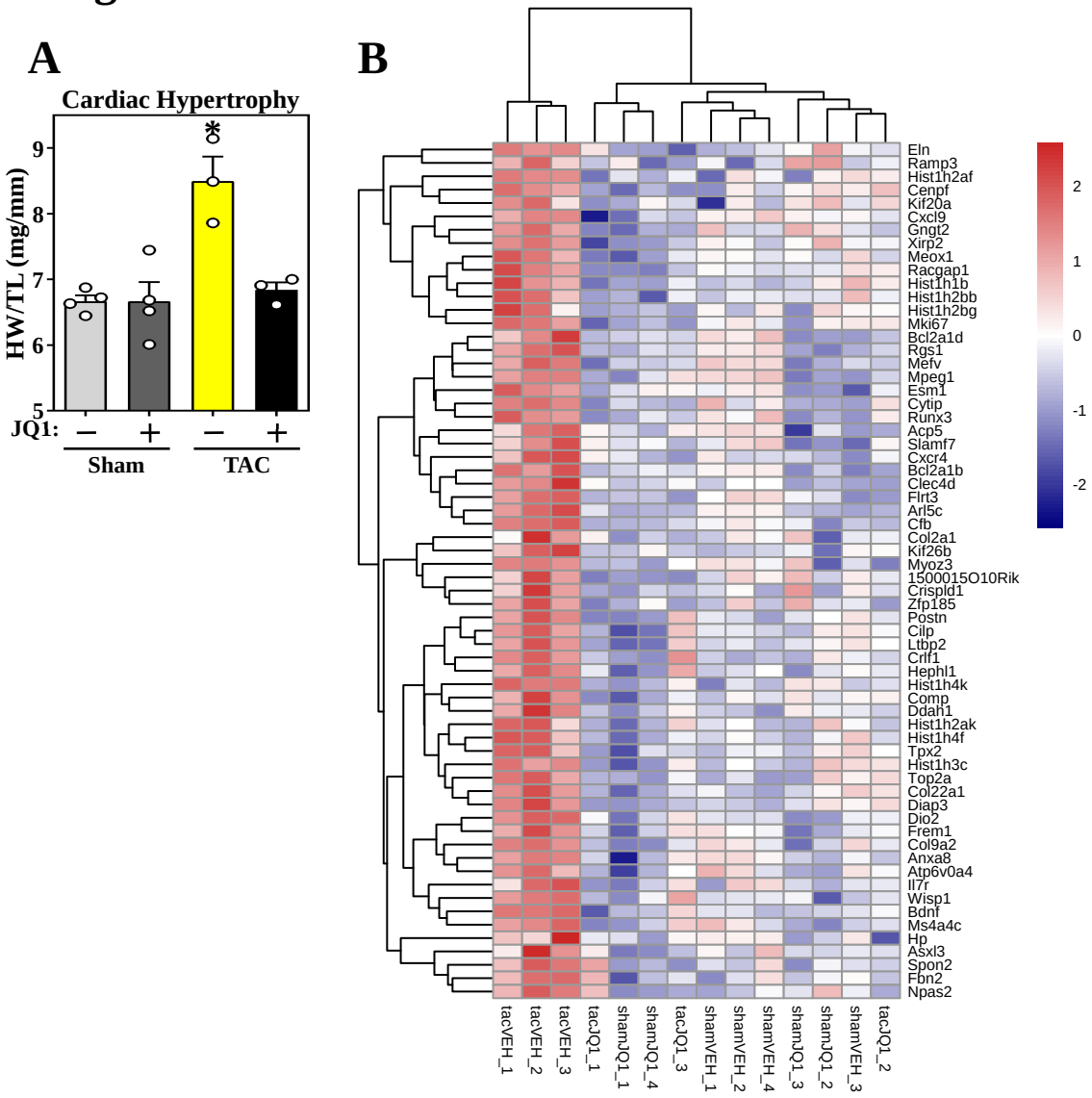

Online Figure IV

A Induced by TGF-β: Mass spec vs. RNA-seq

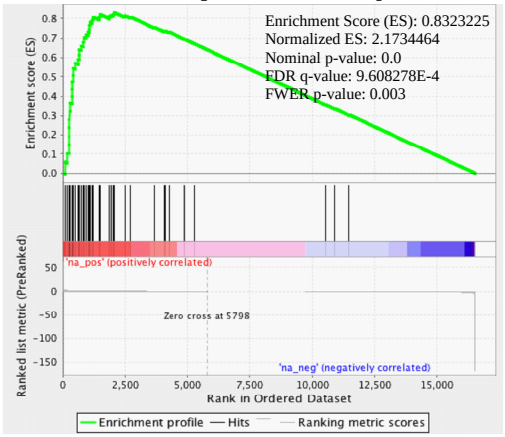

UDP-N-Acetyl-D-Glucosamine Biosynthesis II p=3.23 E-5
L Cysteine Degradation II p=1.49 E-03
Acute Phase Response Signaling p=2.39 E-03
Sulfate Activation of Sulfonation p=2.98 E-03
Cysteine Biosynthesis/Homocysteine degradation p=2.98 E-03

B Repressed by TGF-β: Mass spec vs. RNA-seq

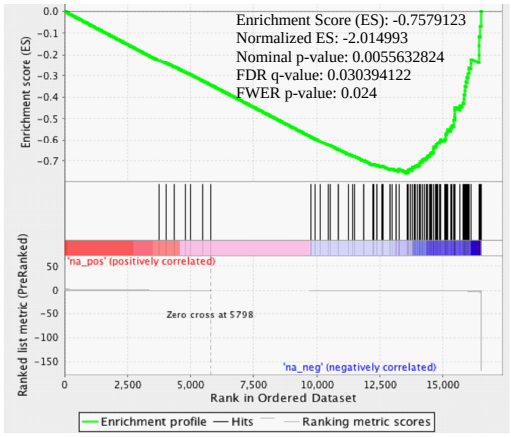

Apelin Adipocyte Signaling Pathway p=1.81 E-06
Glutathione Redox Reactions I p= 3.00 E-05
Tight Junctions Signaling p=6.68 E-05
LPS/IL-1 mediated inhibition of RXR p=2.57 E-04
Aryl Hydrocarbon Receptor Signaling p=4.76 E-04

C Induced by TGF-β (RNA-seq) vs. Induced by TAC (RNA-seq)

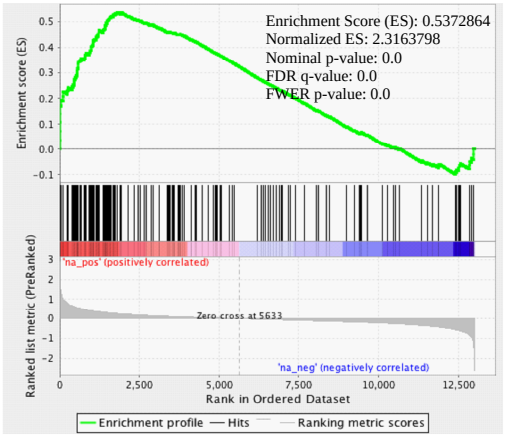

Remodeling of Epithelial Adherens Junctions p=1.11 E-03
UDP-D-Xylos and UDP-D-Glucuronate Biosynthesis p=5.87 E-03
Alanine Degradation III p=5.87 E-03
Alanine Biosynthesis II p=5.87 E-03
Phagosome Maturation p=9.5 E-03

D Repressed by TGF-β (RNA-seq) vs. Repressed TAC (RNA-seq)

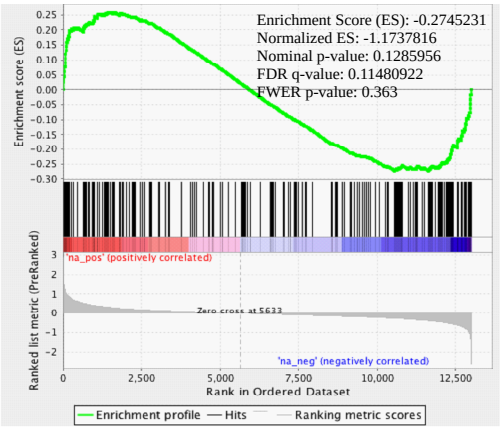

Apelin Adipocyte Signaling Pathway p=1.22 E-03
Glutathione Redox Reactions I p=1.80 E-03
Glutamine Biosynthesis I p=2.62 E-03
LPS/IL-1 mediated inhibition of RXR Function p=2.84 E-03
Glutathione mediated detoxification p=3.19 E-03

E Induced by TGF-β (Mass spec) vs. Induced by TAC (RNA-seq)

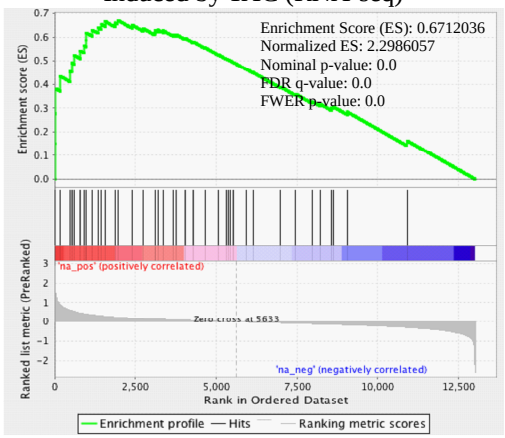

Retinoate Biosynthesis II p=3.07 E-3
UDP-N-Acetyl-D-Glucosamine Biosynthesis II p=4.61 E-03
Parkinsons Signaling p=1.22 E-02
Visual Cycle p=1.53 E-02
Retinoate Biosynthesis p=2.58 E-02

F Repressed by TGF-β (Mass spec) vs. Repressed by TAC (RNA-seq)

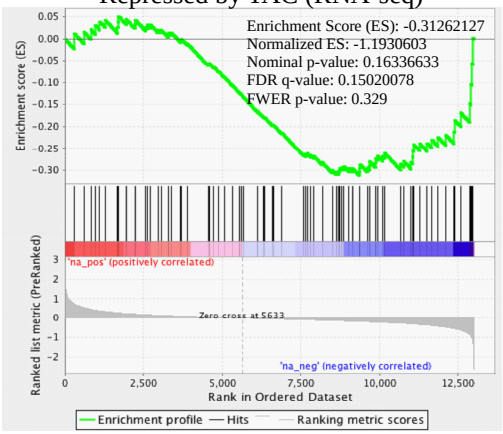

Apelin Adipocyte Signaling Pathway p=1.4 E-04
Oxidative Ethanol Degradation III p=3.2 E-04
Glutatione Redox Reactions I p=4.2 E-04
Ethanol Degradation IV p=4.56 E-04
Aryl Hydrocarbon Receptor Signaling p=7.72 E-04

G Altered by TGF-β and TAC (RNA-seq) and Normalized by JQ1

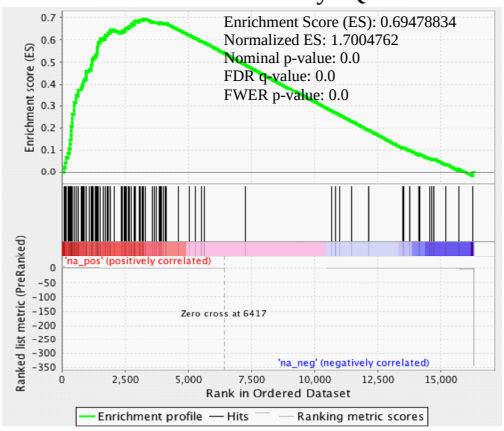

Toll-like Receptor Signaling p=4.28E-06
Role of Macrophages, Fibroblasts and Endothelial Cells in Rheumatoid Arthritis p=7.86E-05
Cell Cycle: G2/M DNA Damage Checkpoint Regulation p=5.05E-04
Role of Osteoblasts, Osteoclasts and Chondrocytes in Rheumatoid Arthritis p=9.17E-04
GADD45 Signaling p=1.63E-03

Online Figure V

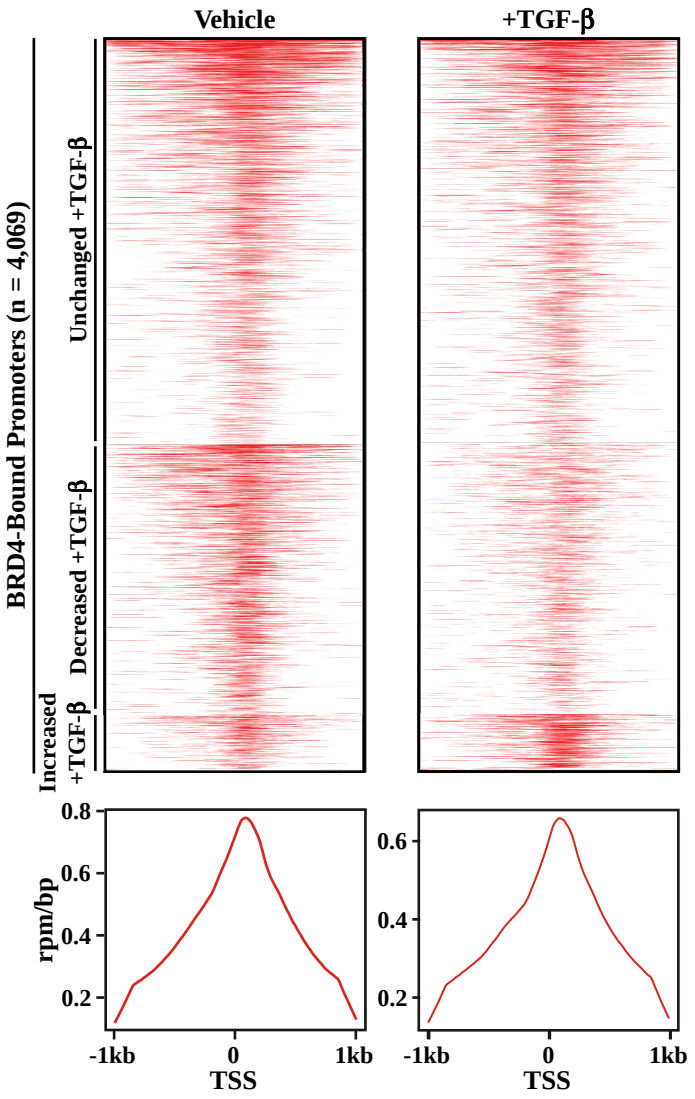

Online Figure VI

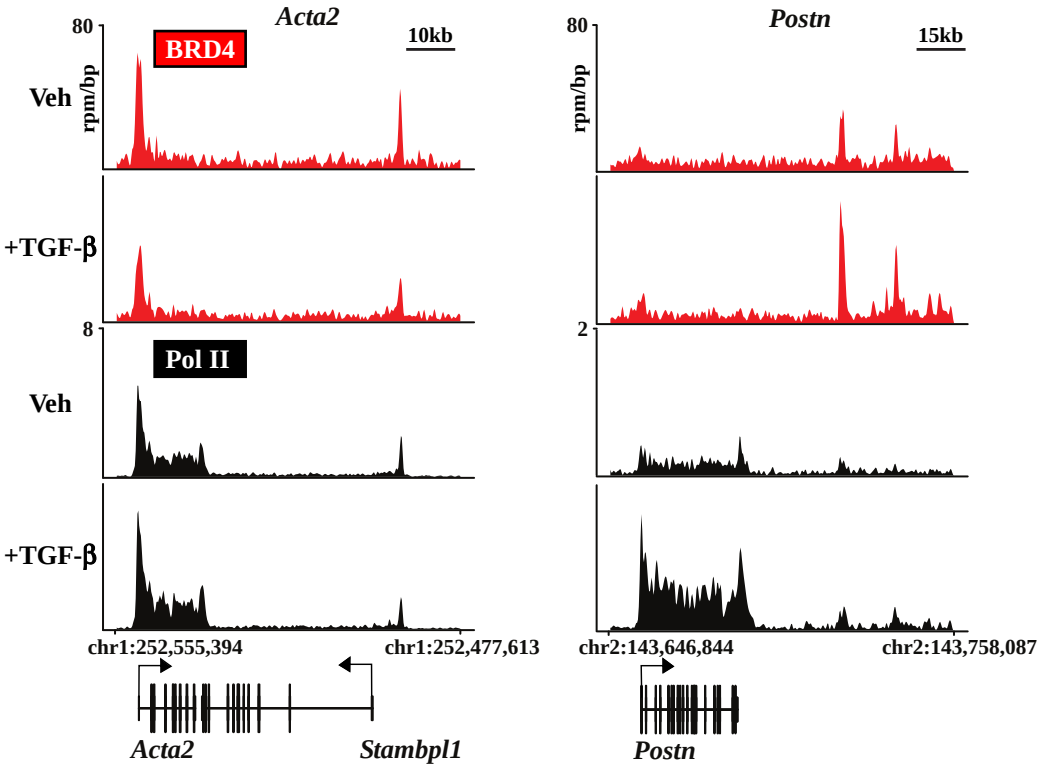

Tweet

Epigenomic analyses establish a critical role for the BRD4 chromatin reader protein in the control of cardiac fibroblast activation and fibrosis of the heart.